Published in final edited form as:
J Mol Cell Cardiol. 2013 November ; 64: . doi:10.1016/j.yjmcc.2013.08.010.

Dynamics of the Late Na^+ current during cardiac action potential and its contribution to afterdepolarizations

Balazs Horvath, M.D. Ph.D.[1,2], **Tamas Banyasz, M.D. Ph.D.**[1,2], **Zhong Jian, Ph.D.**[1], **Bence Hegyi, M.D.**[2], **Kornel Kistamas, M.S.C.**[2], **Peter P. Nanasi, M.D. Ph.D.**[2], **Leighton T. Izu, Ph.D.**[1], and **Ye Chen-Izu, Ph.D.**[1,3,4]

[1]Department of Pharmacology, University of California, Davis, USA

[2]Department of Physiology, University of Debrecen, MHSC, Debrecen, Hungary

[3]Department of Biomedical Engineering, University of California, Davis

[4]Department of Internal Medicine, Division of Cardiology, University of California, Davis

Abstract

The objective of this work is to examine the contribution of late Na^+ current ($I_{Na,L}$) to the cardiac action potential (AP) and arrhythmogenic activities. In spite of the rapidly growing interest toward this current, there is no publication available on experimental recording of the dynamic $I_{Na,L}$ current as it flows during AP with Ca^{2+} cycling. Also unknown is how the current profile changes when the Ca^{2+}-calmodulin dependent protein kinase II (CaMKII) signaling is altered, and how the current contributes to the development of arrhythmias. In this study we use an innovative AP-clamp Sequential Dissection technique to directly record the $I_{Na,L}$ current during the AP with Ca^{2+} cycling in the guinea pig ventricular myocytes. First, we found that the magnitude of $I_{Na,L}$ measured under AP-clamp is substantially larger than earlier studies indicated. CaMKII inhibition using KN-93 significantly reduced the current. Second, we recorded $I_{Na,L}$ together with I_{Ks}, I_{Kr}, and I_{K1} in the *same* cell to understand how these currents counterbalance to shape the AP morphology. We found that the amplitude and the total charge carried by $I_{Na,L}$ exceed that of I_{Ks}. Third, facilitation of $I_{Na,L}$ by Anemone toxin II prolonged APD and induced Ca^{2+} oscillations that led to early and delayed afterdepolarizations and triggered APs; these arrhythmogenic activities were eliminated by buffering Ca^{2+} with BAPTA. In conclusion, $I_{Na,L}$ contributes a significantly large inward current that prolongs APD and unbalances the Ca^{2+} homeostasis to cause arrhythmogenic APs.

Keywords

Na^+ channel; late Na^+ current; action potential; calcium; myocyte; cardiac; arrhythmia

Correspondence: Ye Chen-Izu, Ph.D., Assistant Professor, Department of Pharmacology, University of California, Davis, 2221 Tupper Hall, 451 Health Science Drive, Davis, CA 95616, USA, Phone: (530) 752-3232, YCHENIZU@UCDAVIS.EDU, Tamas Banyasz, M.D. Ph.D., Associate Professor, Department of Physiology, University of Debrecen, BANYASZ.TAMAS@MED.UNIDEB.HU.

Conflict of Interest: none.

Disclosures: None.

1. Introduction

The late Na^+ current ($I_{Na,L}$) influences the cardiac action potential (AP) repolarization [1–5], participates in Na^+-Ca^{2+} homeostasis of cardiac cells [6–13], and can promote arrhythmogenic activities [13–17]. This tiny, persistent Na^+ current has received increasing attention since its selective inhibition eliminated arrhythmogenic APs [5, 15–17], but electrophysiological recording of the $I_{Na,L}$ current has been technically challenging. Our current knowledge on $I_{Na,L}$ is mostly based on the voltage-clamp data obtained under simplified conditions (rectangular voltage pulse, ion substitutions, exogenous Ca^{2+} buffer etc.). The data was then used in model simulations to predict the dynamic profile of the current during AP in order to understand its role in shaping the AP. Although this approach has contributed valuable knowledge, using standard voltage-clamp technique to study $I_{Na,L}$ suffers a great limitation due to a unique feature of the Na^+ channel called *non-equilibrium gating*. Clancy et al. [13] first discovered an enhancement of $I_{Na,L}$ under a repolarizing voltage ramp (instead of a rectangular voltage step), and this can be explained by a fast recovery of the Na^+ channel from inactivated state and reactivation during repolarization ramp (non-equilibrium condition). The non-equilibrium gating gives rise to a large portion of $I_{Na,L}$ and, importantly, this portion of the current cannot be activated by rectangular pulse voltage-clamp protocol [13, 15]. The divergent $I_{Na,L}$ profiles reported in previous literature highlight the complexity in Na^+ channel gating and the necessity to directly record $I_{Na,L}$ under AP-clamp, because dynamic changes of the membrane potential during AP would significantly influence I_{Na}. In this study we use a special version of AP-clamp technique called *self* AP-clamp (sAP-clamp) [18–20] to directly record the $I_{Na,L}$ during AP in the guinea pig ventricular myocytes under a triad of conditions: use the cell's own steady state AP as the voltage command; keep physiological ionic compositions in the internal and external solutions; and preserve the intracellular Ca^{2+} cycling. The goal is to visualize and analyze $I_{Na,L}$ as it flows during cardiac AP under physiological conditions in order to understand its contribution to shaping cardiac APs.

Voltage gated Na^+ channels are known to be regulated by Ca^{2+}, calmodulin (CaM), and Ca^{2+}-CaM dependent protein kinases II (CaMKII); each of these molecules also individually and collectively modulates $I_{Na,L}$ [21–23]. Previous studies exploring the individual elements of this complex regulation reported conflicting results. For example, Wingo et al. proposed that Ca^{2+} modulates Na^+ current by directly binding to the EF-hand motif in the C-terminus [24], but different studies provided evidence against this notion [25, 26]. Tan et al. showed that CaM enhances slow inactivation of I_{Na} [27], and Kim et al suggested that CaM binding minimizes the sustained channel activity [25]. The current consensus is that Ca^{2+}-CaM-CaMKII signaling facilitates cardiac Na^+ current [23]. However, the simplified conditions used in traditional voltage-clamp experiments make it difficult to determine the integrated effects of Ca^{2+}-CaM-CaMKII signaling pathway on modulating the I_{Na} during AP. Furthermore, many previous studies used rectangular pulse voltage-clamp protocol and the non-equilibrium gating of Na^+ channel was absent from those data [28–30]. In this study we use the sAP-clamp technique to directly record the profile of $I_{Na,L}$ during the AP with Ca^{2+} cycling, after Ca^{2+} overloading or chelation, and following CaMKII inhibition. The results provide the first experimental measure of CaMKII modulation of the dynamic $I_{Na,L}$ during cardiac AP. We also further investigated changes in the AP profile when $I_{Na,L}$ is facilitated by Anemone toxin II (ATX-II) to explore the role of $I_{Na,L}$ in arrhythmogenesis.

2. Methods

All animal handling and laboratory procedures conform to the *Guide for the Care and Use of Laboratory Animals* published by the US National Institutes of Health, and to our Institutional Animal Care and Use Committee approved protocols. Chemicals and reagents

were purchased from Sigma-Aldrich if not specified otherwise. Tetrodotoxin (TTX) and ATX-II were from EMD Chemicals. E4031 and Chromanal-293B were from TOCRIS. All experiments were conducted at 36±0.2 °C.

2.1. Cell isolation

Hartley guinea pig (male, 3–5 months old, purchased from Charles River Laboratories USA) were first injected with heparin (800u, I.P.) and then anesthetized with nembutal (100 mg/kg, I.P.). After achieving deep anesthesia a standard enzymatic technique was used to isolate ventricular myocytes at 37 °C. Hearts were mounted on a Langendorff system, and retrogradely perfused for 3–5 minutes with oxygenated solution containing (in mmol/l): NaCl 135, KCl 5.4, $CaCl_2$ 1, $MgCl_2$ 1, NaH_2PO_4 0.3, HEPES 10, glucose 10; pH=7.2. Then a Ca^{2+}-free solution containing (in mmol/l): NaCl 135, KCl 5.4, $MgCl_2$ 1, $NaHPO_4$ 0.3, HEPES 10, glucose 10, EGTA 0.05 (pH=7.2) was perfused for 3 minutes to stop the beating of the heart. Next, a solution containing (in mmol/l): NaCl 135, KCl 5.4, MgCl2 1, NaHPO4 0.3, HEPES 10, glucose 10), and supplemented with 0.6 mg/ml type II collagenase (298 U/mg; Worthington, USA) and 0.05 mg/ml protease type XIV (Sigma, USA) was perfused to enzymatically dissociate cells. After perfusion, the left ventricle was minced and further incubated in the above solution for 40, 60, 80 minutes at 37 °C. Cells were then harvested and stored in a modified Tyrode solution (BTY) containing (in mmol/l): NaCl 120, KCl 5, $CaCl_2$ 2, $MgCl_2$ 1, HEPES 10, $NaHCO_3$ 25, Glucose 10, pH=7.3 (adjusted using NaOH) and osmolarity=295–300 mmol/kg.

2.2. Electrophysiology

Cells were placed in a temperature controlled plexiglass chamber (Cell Microsystems, USA) and superfused with BTY solution (see above). Electrodes were fabricated from borosilicate glass (World Precision Instruments, USA) with tip resistances of 2–2.5 MΩ when filled with internal solution. To preserve the normal Ca^{2+} cycling during AP, we used the internal solution containing (in mmol/l): K-Aspartate 100, KCl 45, Mg-ATP 3, HEPES 5, cAMP 0.1, phosphocreatine dipotassium salt 10, Fura-2 K^+ salt 0.02 (pipette loading), with pH=7.3 (adjusted using KOH) and osmolarity = 284–288 mmol/kg. To buffer intracellular Ca^{2+} to 100 nM (MaxChalator calculation) we used the internal solution containing (in mmol/l): K-Aspartate 74, KCl 43, KOH 25, Mg-ATP 3, HEPES 5, cAMP 0.1, phosphocreatine dipotassium salt 10, BAPTA 10, $CaCl_2$ 2.48, Fura-2 K^+ salt 0.02, with pH=7.3.

sAP-clamp Sequential Dissection experiments were conducted as described in our previous publication [19]. Basic steps include: (1) Record the cell's steady state AP under I-clamp (I=0) at 1 Hz pacing frequency. (2) Apply this AP onto the same cell as the voltage command under V-clamp at 1 Hz. The net current output, I_{BG} should be zero. (3) Isolate the current of interest by using its specific blocker to remove it from the net current output, I_{drug}. (4) The current of interest is then obtained by subtraction: $I = I_{BG} - I_{drug}$. (5) Next, isolate the 2nd current of interest by applying the 2nd channel blocker, and then obtained the 2nd current by subtraction: $I_2 = I_{drug1} - I_{drug2}$. Repeat (5) to isolate the 3rd, the 4th, and more currents by sequentially adding the specific blocker for each channel. The currents were recorded after they had reached steady-state. The following blockers used for dissecting out the currents: 10 μM chromonal-293B for I_{Ks}, 1μM E4031 for I_{Kr}, and 50 μM Ba^{2+} for I_{K1}.

Current-clamp experiments were conducted to record action potentials (APs). Cells were stimulated with supra-threshold depolarizing pulses (2 ms duration) delivered via the patch pipette. APs were recorded at various pacing frequencies. After reaching steady state at each frequency, at least 50 consecutive APs were recorded to examine the average behavior. The frequency series were first recorded under control condition (in BTY), and then repeated after treatment with 10, 30 and 100 nM of ATX-II.

2.3. Measurement of intracellular Ca^{2+} concentration, $[Ca^{2+}]_i$

Cells were loaded with 20 μM Fura-2 K^+ salt (Invitrogen, USA) through the patch pipette for simultaneous recording of the electrical $sig_{Na,L}$ and the Ca^{2+} $sig_{Na,L}$ in the same cell. $[Ca^{2+}]_i$ was measured using IonOptix system (Ionoptix, USA) with dual excitation at 340 nm and 380 nm, and emission at >510 nm (long pass filter). The background fluorescence was measured after tight seal formation. After subtracting the background signal, the fluorescence ratio (F340/F380) was then used to measure $[Ca^{2+}]_i$ as described previously [31].

2.4. Ca^{2+} loading of ventricular myocytes

The myocytes were stimulated at 1 Hz under current-clamp mode during the entire Ca^{2+} loading and washing procedure below. To increase the cytosolic Ca^{2+} concentration the cells were superfused with a modified Tyrode's solution with lower Na^+ concentration (110 mM instead of 145 mM, osmolarity was compensated with NMDG) for 10 minutes (Ca^{2+} loading), and then returned to BTy solution for 5 minutes (washing). This protocol resulted in significant increases in the diastolic Ca^{2+} concentration as measured by Fura-2 at the end of the washing procedure. Then the sAP-clamp experiments were immediately carried out to measure the $I_{Na,L}$ under high Ca^{2+} load condition.

2.5. Statistical Analysis

The numerical values are presented as Mean ± Standard Error of Mean (SEM) in figures if not noted otherwise. Paired or unpaired Student's t-test with equal variance (after using F-test to confirm equal variance) and 2 tails is used to evaluate the difference in the mean values, and the difference between two groups is deemed significant if $p<0.05$.

3. Results

3.1. Profile of $I_{Na,L}$ under sAP-clamp with Ca^{2+} cycling

In order to study the magnitude and time course of $I_{Na,L}$ during AP in the ventricular myocyte, we used sAP-clamp technique to directly record $I_{Na,L}$ under a triad of conditions that mimic in situ environment: during the cell's steady state AP, in a physiological ionic milieu (no ion substitution), and with intracellular Ca^{2+} cycling (no exogenous Ca^{2+} buffer). Fig.1A shows a set of Na^+ currents obtained as TTX-sensitive currents under sAP-clamp. Notice that while the increasing TTX concentrations (between 0.3–30 μM,) inhibit larger and larger fraction of the plateau current the profile of the Na^+ current keeps the same shape, indicating that TTX is a highly specific blocker in this concentration range. The TTX-sensitive current displayed a fast component that declined within 20 ms after the AP upstroke and a slow component that turned around to increase during the AP plateau and persisted throughout the AP; these two components demonstrate that TTX blocked both the fast and the late Na^+ current. The slow current seen from the turning point to the end of AP is late Na^+ current, $I_{Na,L}$.

$I_{Na,L}$ recorded under sAP-clamp displays a strikingly different profile from the small and monotonically decaying current seen under rectangular pulse voltage-clamp; the late Na^+ current is now clearly separated from the fast Na^+ current. As shown in Fig.1A, $I_{Na,L}$ was a small current at AP phase-1, increased gradually during phase-2 and -3, reached a peak at APD50, and then declined rapidly. Fig.1B&C demonstrate TTX dose-response of the peak (Fig.1B) and the mid plateau (Fig.1C) values of $I_{Na,L}$; the data were fitted to Hill equation with Hill coefficient of 1 and IC50 of 0.94 μM and 0.95 μM, respectively. Hence, using 10–30 μM TTX was sufficient for dissecting out the full measure of $I_{Na,L}$. The peak current density of $I_{Na,L}$ under sAP-clamp reached 0.78±0.07 A/F, demonstrating a surprisingly

larger current. The instant I-V relationship of $I_{Na,L}$ shows a bell-shaped curve with the peak current occurring at −15.3±4.6 mV (Fig.1D). A strong correlation also exists between the time to peak $I_{Na,L}$ and APD50 (Fig.1E).

3.2. Modulation of $I_{Na,L}$ during AP by Ca^{2+} and CaMKII

We further investigate how the $I_{Na,L}$ profile during AP changes by increasing or decreasing the intracellular Ca^{2+}, and by CaMKII inhibition. When the cytosolic Ca^{2+} concentration was clamped to 100 nM by using BAPTA, the AP was significantly lengthened and the $I_{Na,L}$ recorded under sAP-clamp was significantly enlarged (Fig.2A). At the beginning, the $I_{Na,L}$ in the Ca^{2+} clamped cell progressed at the same rate as in the control, but it continues to rise as the AP is lengthened and thus reached a higher peak. The instant I-V relationship for the control and the Ca^{2+} buffered cell showed difference in magnitude but no shift in the voltage dependency. The $I_{Na,L}$ current density was significantly increased during AP (Fig.2C) and the total amount of Na inflow carried by $I_{Na,L}$ was tripled in Ca^{2+} buffered cells (Fig.2D). Therefore, the lengthening of AP and elevation of plateau voltage under the low Ca^{2+} condition facilitates the $I_{Na,L}$ during AP.

Since $I_{Na,L}$ was increased by chelating Ca^{2+}, next we investigate whether increasing cytosolic Ca^{2+} would have the opposite effect. We used a Ca^{2+} loading procedure (see Method #2.4) to increase the amplitude and the baseline of the Ca^{2+} transient during AP, and recorded $I_{Na,L}$ under sAP-clamp. Contrary to the expectation, the profile of $I_{Na,L}$ during AP and the I-V relationship did not decrease but is similar to that of the control (Fig.2A & 2B); the current density and the total charge carried by the current are also similar to the control (Fig.2C & 2D). These data suggest two possibilities: one is that the $I_{Na,L}$ sensitivity to Ca^{2+} might be already saturated at the control condition so there is no further change with Ca^{2+} overload; another is that the $I_{Na,L}$ might not be sensitive to Ca^{2+} and the facilitation of $I_{Na,L}$ in Ca^{2+} buffered cells solely results from the altered voltage profile of AP.

Furthermore, we investigated the effect of CaMKII inhibition on the $I_{Na,L}$ profile during AP. The cells were treated with 1 μM KN-93 in bath while being paced at 1 Hz at current-clamp mode for 10 minutes. KN-93 treatment reduced the magnitude of $I_{Na,L}$ during AP (Fig.2A) without significantly altering the I-V relationship (Fig.2B). The mid-plateau current magnitude and the peak amplitude were significantly decreased (Fig.2C). Nevertheless, the total amount of charge carried by the current during the AP was not significantly different from the control (Fig.2D), due to a lengthening of the APD_{90} by KN93 treatment (244.2±18.2ms vs. 204.7±9.2ms, $p<0.05$) that compensated for the decreased current amplitude.

To investigate the non-equilibrium gating, we use a Triangulation Factor (defined as $TF=APD_{90}/APD_{20}$) to characterized the membrane voltage change during AP. As shown in Fig.2E, BAPTA decreased TF as the AP lengthened and hence increased the peak $I_{Na,L}$ amplitude. Low Na treated cells had similar TF and the peak $I_{Na,L}$ as the control. KN93 treatment increased TF and reduced the peak $I_{Na,L}$. In fact, the peak $I_{Na,L}$ current amplitude displays a tight positive correlation with TF (Pearson's r value, r=0.921) under all experimental conditions tested, demonstrating a prominent influence of the non-equilibrium gating on the $I_{Na,L}$ current amplitude during AP.

3.3. $I_{Na,L}$ contributes significantly to the AP plateau

To understand the role of $I_{Na,L}$ in shaping AP we investigated how the inward charge movement through $I_{Na,L}$ is counterbalanced by the outward charge movement through K^+ currents. We recorded the I_{Ks}, I_{Kr} I_{K1}, and $I_{Na,L}$ from the same cell using the sAP-clamp Sequential Dissection method (Fig.3A). Under control condition, the peak current density of

$I_{Na,L}$ is higher than that of I_{Ks} but lower than that of I_{Kr} or I_{K1}. The $I_{Na,L}$ peaks at the end of phase-2 of AP, about the same time when I_{kr} and I_{k1} increase rapidly, but the magnitudes of the K^+ currents become much larger and thus resulting in an acceleration of repolarization in the phase-3 of AP(Fig 3A). Surprisingly, the amount of inward charges carried by $I_{Na,L}$ during the AP is comparable to the outward charges carried by each individual K^+ current.

Facilitation of $I_{Na,L}$ with 10 nM ATX-II resulted in a robust increase in $I_{Na,L}$ magnitude without altering the K^+ currents (Fig.3B & 3C). Moreover, ATX-II treatment further increased the total charge carried by $I_{Na,L}$ which significantly exceeds the outward charges carried by any individual K^+ current (Fig.3D). The voltage dependence of $I_{Na,L}$ shown in the instant I-V relationship was not altered (Fig.3E). Facilitation of $I_{Na,L}$ by ATX-II resulted in significant lengthening of AP (APD_{90} = 212.0±19.9ms ATX-II vs. 192.5±15.6ms control; Fig.3B) without altering the voltage dependence of $I_{Na,L}$. A tight positive correlation is found between the net charge carried by $I_{Na,L}$ and the AP duration (Fig.3F). These data reveals a significant contribution of the $I_{Na,L}$ to shaping the AP morphology, and upregulation of $I_{Na,L}$ can give rise to long APD.

3.4. Upregulation of $I_{Na,L}$ leads to arrhythmogenic APs

To further investigate the role of $I_{Na,L}$ in arrhythmogenesis, we recorded the action potentials under current-clamp mode and studied the effect of upregulating $I_{Na,L}$ using ATX-II. Our data show that ATX prolonged APD and induced arrhythmogenic APs in a dose-dependent manner (Fig.4A). While APD_{20} was not significantly altered by ATX-II in the range of 10–100 nM, APD_{35}, APD_{50} and APD_{90} were greatly lengthen by ATX-II at 10 nM and above (Fig.4B). Early afterdepolarizations (EADs) emerged with 30–100 nM ATX-II treatment; EADs often occurred during early plateau phase, within 400–500 ms after the upstroke of AP. In addition to EADs, delayed afterdepolarizations (DADs) and triggered APs (TAPs) also emerged in 100 nM ATX-II in the same cell (Fig.4C), suggesting a common origin for these different forms of arrhythmogenic APs.

3.5. Spontaneous Ca^{2+} release from SR mediates $I_{Na,L}$ induced arrhythmogenic APs

We hypothesized that ATX-II induced EADs are caused by Ca^{2+} release from SR (which also causes DADs and TAPs), rather than by reactivation of the L-type Ca^{2+} current during prolonged AP. To test this hypothesis we simultaneously recorded AP and the intracellular Ca^{2+} concentration ($[Ca^{2+}]_i$) using Fura-2 under the current-clamp mode. Fig.5A demonstrates that EADs occurred in concomitant with intracellular Ca^{2+} oscillations. As a tell-tale sign, the first spontaneous Ca^{2+} wave after the paced systolic Ca^{2+} transient always rises *before* the membrane voltage turns upward to form EAD. These data suggest that the Ca^{2+} wave drives the inward Na^+/Ca^{2+} exchange current (forward mode) to give rise to EAD. In support of this notion, eliminating Ca^{2+} oscillations using BAPTA also abolished EADs (Fig.5B). Recall that BAPTA treatment also prolonged APD (Fig.2B) which should increase the reactivation of L-type Ca^{2+} current. Hence the cause of ATX-II induced EADs is not reactivation of L-type Ca^{2+} current but spontaneous Ca^{2+} release from SR. In further support of this notion, the systolic Ca^{2+} transient was higher in ATX-II treated cells than in the control (Fig.5C), demonstrating a higher SR load that would facilitate spontaneous Ca^{2+} release from SR. In relating to arrhythmogenic APs, $I_{Na,L}$ upregulation by 100 nM ATX-II induced long APD and EADs in all cells examined, and also DADs and TAPs in some cells (Fig.5D). In contrast, Ca^{2+} buffering by BAPTA prolonged APD, but eliminated EAD, DAD and TAP. As a final confirmation for the role of Ca^{2+} oscillation in generating EAD, we conducted a self-controlled experiment in the same cell. As shown in Fig.5E, we first used perforated patch technique with the pipette solution containing 10 mM BAPTA and recorded EADs evoked by 100 nM ATX-II treatment; the Ca^{2+} oscillations were behind the EAD generation since the BAPTA could not get into the cell in the perforated patch

configuration (Amphotericin was used to form small perforations in the cell membrane patch). Then we ruptured the membrane patch to form a ruptured whole-cell configuration to allow BAPTA diffusion into the cytosol; this eliminated Ca^{2+} oscillation and EAD but did not shorten APD. Therefore, $I_{Na,L}$ directly contribute to lengthening APD, but the effect of $I_{Na,L}$ on evoking EAD, DAD, and TAP is Ca^{2+} dependent through altered Na^+ – Ca^{2+} homeostasis.

4. DISCUSSION

In order to understand the contribution of $I_{Na,L}$ to the normal and arrhythmogenic APs, we have recorded $I_{Na,L}$ during the cell's steady state AP in a physiological ionic milieu with Ca^{2+} cycling, while the cell was undergoing excitation-contraction at body temperature. To our best knowledge, this is the first time $I_{Na,L}$ has been recorded under these conditions designed to closely mimic the physiological environment. Several pioneering studies used different variance of AP-clamp technique to measure $I_{Na,L}$ [32–35]. However, all of them used AP waveforms recorded from other cells or reconstructed from model and therefore caused the measured current to deviate from the original current naturally flowing under the cell's own AP. Moreover, the earlier AP-clamp experiments also used ion substitution (replacing Na^+ with Cs^+ or K^+ with TEA) and exogenous Ca^{2+} buffer which, albeit useful for dissecting the biophysical properties of the channel, also deviate from physiological conditions and introduce some artifacts. The present sAP-clamp study was designed to directly record the $I_{Na,L}$ following under the cell's own AP during excitation-contraction coupling under physiological conditions. The data so obtained revealed novel findings on the dynamics of $I_{Na,L}$ during AP and its role in arrhythmogenesis as discussed below.

4.1. Non-equilibrium gating is a chief factor determining the profile of $I_{Na,L}$ during AP

Our data show that $I_{Na,L}$ has a *saddle-like* profile during the AP in guinea pig ventricular myocyte (Fig.1A): after the fast Na^+ current declines during phase-1, the late Na^+ current ($I_{Na,L}$) takes a turn to increase during phase-2, reaches a peak at about APD_{50}, and then rapidly declines during phase-3, and returns to baseline at phase-4. First of all, note that the profile of $I_{Na,L}$ recorded with rectangular voltage-clamp protocol differs significantly from that $I_{Na,L}$ current seen during AP. The former is invariably triangular in all species due to proliferating inactivation of sodium channels under a constant voltage. The latter, however, was traditionally visualized by computer simulation based on rectangular voltage-clamp data and such simulations often involve simplifications in the model hence still need to be verified experimentally. Our recordings consistently show *saddle-like* $I_{Na,L}$ profile during AP under control condition and also under ATX-II treatment in guinea pig myocytes (Fig. 3A&B). This does not preclude that $I_{Na,L}$ profile could be somewhat different in different species. Saddle-like profile is consistent with the simulation results from some models (canine [36], human [37], and guinea pig ventricular myocyte [38], and recombinant Na^+ channel expressed in cell line 293 [13]), but differ from some other model simulations predicting *triangle-like* profile during AP (canine [33]; guinea pig [32]). Thus, our experimental data confirm those models, where $I_{Na,L}$ accumulates during the AP plateau giving a peak before terminal repolarization.

The profile of $I_{Na,L}$ is shaped by several mechanisms including 'window current' and 'non-equilibrium gating' [16]. A 'window current' occurs when ion channels reactivate in a voltage range where the steady-state activation and inactivation curves overlap. The window current voltage range for the Na^+ channel is quite negative (e.g. −80 mV to −50 mV) [39]. The AP plateau, however, falls in the positive voltage range before repolarization. Hence the window current should be negligible during plateau. On the other hand, repolarizing voltage ramp was found to facilitate $I_{Na,L}$ [13], and this phenomenon was termed non-equilibrium

gating. Therefore, a steep repolarization in AP is expected to boost $I_{Na,L}$. Moreover, non-equilibrium gating is not detectable by the rectangular pulse voltage-clamp experiments that measure steady-state currents [13]. Therefore, earlier models based on steady-state currents would miss the non-equilibrium gating and produce a triangle-like $I_{Na,L}$ profile without the saddle-like profile obtained in our sAP-clamp experiment. Our data is consistent with non-equilibrium gating, and provide a realistic measure of the $I_{Na,L}$ during dynamic changes of the membrane potential during AP for fine-tuning future models.

4.2. Ca^{2+} dependent modulation of $I_{Na,L}$ during AP

Ca^{2+} was proposed to modulate $I_{Na,L}$ by direct and indirect mechanisms. Direct Ca^{2+} binding to hH1 domain of sodium channel was shown to induce a rightward shift in the steady state inactivation increasing the availability of channels at more positive potentials [24], therefore buffering cytosolic Ca^{2+} should reduce Na^+ current. Inhibition of CaM-CaMKII pathway showed divergent effects on $I_{Na,L}$ in different previous reports. In our experiments when BAPTA was used to buffer cytosolic Ca^{2+}, The APD and plateau height were significantly increased, which give rise to substantially increased $I_{Na,L}$ during the AP (Fig 2). The positive correlation between the triangulation factor of AP and the peak amplitude of $I_{Na,L}$ further supports the conclusion that $I_{Na,L}$ is more strongly influenced by the voltage profile during the AP rather than by Ca^{2+}.

CaMKII is known to facilitate Na^+ current [23]. In agreement with this notion, in our experiments CaMKII inhibition using KN-93 reduced $I_{Na,L}$ magnitude throughout the time course of AP and also in the I-V relationship. Meanwhile, increasing Ca^{2+} load did not further increase $I_{Na,L}$, indicating that the Ca^{2+}-CaMKII modulation of $I_{Na,L}$ is already saturated at the control condition. The voltage dependence of the $I_{Na,L}$ recorded under sAP-clamp did not change under all the conditions tested, seen as no horizontal shift in the instant I-V relationship albeit changes in the amplitude of the current density (vertical shift in I-V),. Our data provide, for the first time, a visualization of the impact of Ca^{2+} chelation and CaMKII inhibition on the dynamic profile of $I_{Na,L}$ during the AP.

4.3. The magnitude of $I_{Na,L}$ during AP in comparing to K^+ currents

We found that $I_{Na,L}$ presents a substantial inward current with peak current density of 0.78±0.32 A/F (Mean±SD) and total charge movement of 88.3±43.2 mC/F during the AP in guinea pig ventricular myocytes (Fig.3C&D). For long time it was thought that $I_{Na,L}$ was a *tiny* sustained current during AP, especially in comparing to the fast Na^+ current with much larger amplitude. Now we found that the $I_{Na,L}$ during the AP is surprisingly *large*, even in comparing to the major K^+ currents. The inward charge movement through $I_{Na,L}$ should depolarize the membrane potential, which is counterbalanced by the outward charge movement through K^+ channels. To investigate the interplay of $I_{Na,L}$ and K^+ currents in shaping the AP morphology, we recorded $I_{Na,L}$, I_{Ks}, I_{Kr} and I_{K1} from the same cell. Previously, the relationship between $I_{Na,L}$ and K^+ channels was studied only in model simulations [36], and the ratio between $I_{Na,L}$ and K^+ channels was shown to affect arrhythmogenesis. Now our experimental data show, interestingly, the $I_{Na,L}$ magnitude and time course of seems to mirror that of I_{Ks} (Fig.3A). The peak current density of $I_{Na,L}$ is comparable to I_{Ks}, about 50% of I_{Kr} and 30% of I_{K1} (Fig.3C). The inward charge carried by $I_{Na,L}$ is more than the outward charge carried by any individual K^+ current during the AP cycle, although less than the total charge carried by all three K^+ currents (Fig.3D). Therefore our data reveal that $I_{Na,L}$ is a major determinant of the AP morphology, and significantly contributes to arrhythmogenic AP activities

4.4. Spontaneous Ca^{2+} release from SR mediates $I_{Na,L}$ induced EAD, DAD and TAP

Upregulation of $I_{Na,L}$ is linked to development of arrhythmias in heart failure and other acquired heart diseases [15, 40]. However, the exact role of $I_{Na,L}$ in arrhythmogenesis remained unclear, especially in the genesis of EADs. At least two possible mechanisms have been proposed [16]: one involves reactivation of the L-type Ca^{2+} current; the other involves SR Ca^{2+} overload. In the first mechanism, upregulation of $I_{Na,L}$ prolongs the AP plateau which allows recovery and reactivation of the L-type Ca^{2+} current; then the Ca^{2+} influx disrupts the membrane repolarization to cause EADs [14, 16]. This mechanism emphasizes the window current of the L-type Ca^{2+} channel as the depolarization drive for EADs. Nevertheless, our data show that the first EAD occurred at positive voltages (>10 mV, see Fig.3A) above the Ca^{2+} 'window' current voltage range (−30 mV to 0 mV) [41]; hence, the window current is not responsible for generating the EAD.

In the second mechanism, upregulation of $I_{Na,L}$ increases intracellular Na^+ concentration which causes SR Ca^{2+} overload; SR overload then causes spontaneous Ca^{2+} release from SR which drives forward mode Na^+/Ca^{2+} exchange to depolarize the membrane, resulting in EADs [6, 42, 43]. Our data provide several evidences to support this mechanism. First, the ATX-II treated cells showed elevated systolic Ca^{2+} transient indicating elevated SR load (Fig.5C). Second, the spontaneous Ca^{2+} wave precedes the first EAD (Fig.5A, indicated by dash line); this timing is consistent with increased cytosolic Ca^{2+} drives inward (forward mode) Na^+/Ca^{2+} exchanger to cause EAD. Third, using BAPTA to buffer Ca^{2+} abolished EADs (Fig.5B), although caused a prolonged phase-2; this long plateau feature is clearly different from the EADs driven by Ca^{2+} oscillations (Fig.5A). Therefore, spontaneous Ca^{2+} release from SR is a prerequisite for the generation of EADs. Taken together, our data suggest that spontaneous Ca^{2+} release from SR is a common mechanism underlying $I_{Na,L}$ induced EADs, DADs and TAPs. The common mechanism of EAD and DAD was already proposed in Cs^+ and isoproterenol induced early afterdepolarizations [44, 45] and Udrovinas et al. showed that augmented $I_{Na,L}$ contributes to diastolic Ca^{2+} accumulation [6]. Our data provide experimental evidence to support the common mechanisms of afterdepolarizations proposed in these earlier works.

Acknowledgments

We are grateful to Dr. Robert Hadley (University of Kentucky) for kindly providing the guinea pig cardiac cell isolation protocol. We thank Mr. Shaden Khabbaz for the excellent work in isolating cells.

Funding: This work was supported by the National Institute of Health R01 grant (HL90880) to LTI and YC, NIH R03 grant (AG031944) to YC, American Heart Association National Center Scientist Development Award (0335250N) to YC, European Society of Cardiology Visiting Scientist Award to BH, the Hungarian Research Found OTKA- K101196 and OTKA- K100151 to TB and PPN, and the funds from the University of California to LTI and YC.

References

1. Yuill KH, Convery MK, Dooley PC, Doggrell SA, Hancox JC. Effects of BDF 9198 on action potentials and ionic currents from guinea-pig isolated ventricular myocytes. Br J Pharmacol. 2000; 130:1753–1766. [PubMed: 10952663]
2. Kiyosue T, Arita M. Late Sodium Current And Its Contribution To Action-Potential Configuration In Guinea-Pig Ventricular Myocytes. Circ Res. 1989; 64:389–397. [PubMed: 2536304]
3. Undrovinas AI, Maltsev VA, Sabbah HN. Repolarization abnormalities in cardiomyocytes of dogs with chronic heart failure: role of sustained inward current. Cellular and Molecular Life Sciences. 1999; 55:494–505. [PubMed: 10228563]
4. Belardinelli L, Shryock JC, Fraser H. Inhibition of the late sodium current as a potential cardioprotective principle: effects of the late sodium current inhibitor ranolazine. Heart. 2006; 92:6–14.

5. Maltsev VA, Silverman N, Sabbah HN, Undrovinas AI. Chronic heart failure slows late sodium current in human and canine ventricular myocytes: Implications for repolarization variability. European Journal of Heart Failure. 2007; 9:219–227. [PubMed: 17067855]
6. Undrovinas NA, Maltsev VA, Belardinelli L, Sabbah HN, Undrovinas A. Late sodium current contributes to diastolic cell Ca2+ accumulation in chronic heart failure. The journal of physiological sciences : JPS. 2010; 60:245–257. [PubMed: 20490740]
7. Undrovinas AI, Belardinelli L, Undrovinas NA, Sabbah HN. Ranolazine Improves Abnormal Repolarization and Contraction in Left Ventricular Myocytes of Dogs with Heart Failure by Inhibiting Late Sodium Current. Journal of Cardiovascular Electrophysiology. 2006; 17:S169–S177. [PubMed: 16686675]
8. Fraser H, Belardinelli L, Wang L, Light PE, McVeigh JJ, Clanachan AS. Ranolazine decreases diastolic calcium accumulation caused by ATX-II or ischemia in rat hearts. J Mol Cell Cardiol. 2006; 41:1031–1038. [PubMed: 17027025]
9. Sossalla S, Wagner S, Rasenack EC, Ruff H, Weber SL, Schondube FA, et al. Ranolazine improves diastolic dysfunction in isolated myocardium from failing human hearts--role of late sodium current and intracellular ion accumulation. J Mol Cell Cardiol. 2008; 45:32–43. [PubMed: 18439620]
10. Sossalla S, Maurer U, Schotola H, Hartmann N, Didie M, Zimmermann WH, et al. Diastolic dysfunction and arrhythmias caused by overexpression of CaMKIIdelta(C) can be reversed by inhibition of late Na(+) current. Basic Res Cardiol. 2011; 106:263–272. [PubMed: 21174213]
11. Wasserstrom JA, Sharma R, O'Toole MJ, Zheng J, Kelly JE, Shryock J, et al. Ranolazine antagonizes the effects of increased late sodium current on intracellular calcium cycling in rat isolated intact heart. J Pharmacol Exp Ther. 2009; 331:382–391. [PubMed: 19675298]
12. Hoyer K, Song YJ, Wang DS, Phan D, Balschi J, Ingwall JS, et al. Reducing the Late Sodium Current Improves Cardiac Function during Sodium Pump Inhibition by Ouabain. Journal of Pharmacology and Experimental Therapeutics. 2011; 337:513–523. [PubMed: 21325441]
13. Clancy CE, Tateyama M, Liu H, Wehrens XH, Kass RS. Non-equilibrium gating in cardiac Na+ channels: an original mechanism of arrhythmia. Circulation. 2003; 107:2233–2237. [PubMed: 12695286]
14. Trenor B, Cardona K, Gomez JF, Rajamani S, Ferrero JM Jr, Belardinelli L, et al. Simulation and mechanistic investigation of the arrhythmogenic role of the late sodium current in human heart failure. PLoS One. 2012; 7:e32659. [PubMed: 22427860]
15. Moreno JD, Clancy CE. Pathophysiology of the cardiac late Na current and its potential as a drug target. J Mol Cell Cardiol. 2012; 52:608–619. [PubMed: 22198344]
16. Zaza A, Belardinelli L, Shryock JC. Pathophysiology and pharmacology of the cardiac "late sodium current". Pharmacology & Therapeutics. 2008; 119:326–339. [PubMed: 18662720]
17. Yang T, Atack TC, Stroud DM, Zhang W, Hall L, Roden DM. Blocking Scn10a Channels in Heart Reduces Late Sodium Current and Is Antiarrhythmic. Circ Res. 2012; 111:322–332. [PubMed: 22723299]
18. Banyasz T, Horvath B, Jian Z, Izu LT, Chen-Izu Y. Profile of L-type Ca2+ current and Na+/Ca2+ exchange current during cardiac action potential in ventricular myocytes. Heart Rhythm. 2012; 9:134–142. [PubMed: 21884673]
19. Banyasz T, Horvath B, Jian Z, Izu LT, Chen-Izu Y. Sequential dissection of multiple ionic currents in single cardiac myocytes under action potential-clamp. J Mol Cell Cardiol. 2011; 50:578–581. [PubMed: 21215755]
20. Banyasz T, Fulop L, Magyar J, Szentandrassy N, Varro A, Nanasi PP. Endocardial versus epicardial differences in L-type calcium current in canine ventricular myocytes studied by action potential voltage clamp. Cardiovascular Research. 2003; 58:66–75. [PubMed: 12667947]
21. Maier LS. CaMKII regulation of voltage-gated sodium channels and cell excitability. Heart Rhythm. 2011; 8:474–477. [PubMed: 20887805]
22. Scheuer T. Regulation of sodium channel activity by phosphorylation. Seminars in Cell & Developmental Biology. 2011; 22:160–165. [PubMed: 20950703]
23. Bers DM, Grandi E. Calcium/Calmodulin-dependent Kinase II Regulation of Cardiac Ion Channels. J Cardiovasc Pharmacol. 2009; 54:180–187. [PubMed: 19333131]

24. Wingo TL, Shah VN, Anderson ME, Lybrand TP, Chazin WJ, Balser JR. An EF-hand in the sodium channel couples intracellular calcium to cardiac excitability. Nature Structural & Molecular Biology. 2004; 11:219–225.
25. Kim J, Ghosh S, Liu HJ, Tateyama M, Kass RS, Pitt GS. Calmodulin mediates Ca2+ sensitivity of sodium channels. Journal of Biological Chemistry. 2004; 279:45004–45012. [PubMed: 15316014]
26. Cormier JW, Rivolta I, Tateyama M, Yang AS, Kass RS. Secondary structure of the human cardiac Na+ channel C terminus - Evidence for a role of helical structures in modulation of channel inactivation. Journal of Biological Chemistry. 2002; 277:9233–9241. [PubMed: 11741959]
27. Tan HL, Kupershmidt S, Zhang R, Stepanovic S, Roden DM, Wilde AAM, et al. A calcium sensor in the sodium channel modulates cardiac excitability. Nature. 2002; 415:442–447. [PubMed: 11807557]
28. Deschenes I, Neyroud N, DiSilvestre D, Marban E, Yue DT, Tomaselli GF. Isoform-specific modulation of voltage-gated Na+ channels by calmodulin. Circ Res. 2002; 90:E49–E57. [PubMed: 11884381]
29. Young KA, Caldwell JH. Modulation of skeletal and cardiac voltage-gated sodium channels by calmodulin. J Physiol-London. 2005; 565:349–370. [PubMed: 15746172]
30. Murphy BJ, Rogers J, Perdichizzi AP, Colvin AA, Catterall WA. cAMP-dependent phosphorylation of two sites in the alpha subunit of the cardiac sodium channel. Journal of Biological Chemistry. 1996; 271:28837–28843. [PubMed: 8910529]
31. Chen-Izu Y, Chen L, Banyasz T, McCulle SL, Norton B, Scharf SM, et al. Hypertension-induced remodeling of cardiac excitation-contraction coupling in ventricular myocytes occurs prior to hypertrophy development. Am J Physiol Heart Circ Physiol. 2007; 293:H3301–H3310. [PubMed: 17873027]
32. Chorvatova A, Snowdon R, Hart G, Hussain M. Effects of pressure overload-induced hypertrophy on TTX-sensitive inward currents in guinea pig left ventricle. Mol Cell Biochem. 2004; 261:217–226. [PubMed: 15362507]
33. Murphy L, Renodin D, Antzelevitch C, Di Diego JM, Cordeiro JM. Extracellular proton depression of peak and late Na current in the canine left ventricle. Am J Physiol Heart Circ Physiol. 2011; 301:H936–H944. [PubMed: 21685271]
34. Marangoni S, Di Resta C, Rocchetti M, Barile L, Rizzetto R, Summa A, et al. A Brugada syndrome mutation (p.S216L) and its modulation by p.H558R polymorphism: standard and dynamic characterization. Cardiovasc Res. 2011; 91:606–616. [PubMed: 21705349]
35. Magyar J, Kiper CE, Dumaine R, Burgess DE, Bányász T, Satin J. Divergent action potential morphologies reveal nonequilibrium properties of human cardiac Na channels. Cardiovasc Res. 2004; 64:477–487. [PubMed: 15537501]
36. Flaim SN, Giles WR, McCulloch AD. Contributions of sustained INa and IKv43 to transmural heterogeneity of early repolarization and arrhythmogenesis in canine left ventricular myocytes. American Journal of Physiology - Heart and Circulatory Physiology. 2006; 291:H2617–H2629. [PubMed: 16829642]
37. O'Hara T, Virag L, Varro A, Rudy Y. Simulation of the undiseased human cardiac ventricular action potential: model formulation and experimental validation. PLoS computational biology. 2011; 7:e1002061. [PubMed: 21637795]
38. Sakmann BFAS, Spindler AJ, Bryant SM, Linz KW, Noble D. Distribution of a Persistent Sodium Current Across the Ventricular Wall in Guinea Pigs. Circ Res. 2000; 87:910–914. [PubMed: 11073887]
39. Maltsev VA, Sabbah HN, Higgins RS, Silverman N, Lesch M, Undrovinas AI. Novel, ultraslow inactivating sodium current in human ventricular cardiomyocytes. Circulation. 1998; 98:2545–2552. [PubMed: 9843461]
40. Zaza A. Control of the cardiac action potential: The role of repolarization dynamics. J Mol Cell Cardiol. 2010; 48:106–111. [PubMed: 19666029]
41. Madhvani RV, Xie Y, Pantazis A, Garfinkel A, Qu Z, Weiss JN, et al. Shaping a new Ca2+ conductance to suppress early afterdepolarizations in cardiac myocytes. J Physiol. 2011; 589:6081–6092. [PubMed: 22025660]

42. Burashnikov A, Antzelevitch C. Late-phase 3 EAD. A unique mechanism contributing to initiation of atrial fibrillation. Pacing Clin Electrophysiol. 2006; 29:290–295. [PubMed: 16606397]

43. Pogwizd SM, Schlotthauer K, Li L, Yuan W, Bers DM. Arrhythmogenesis and Contractile Dysfunction in Heart Failure : Roles of Sodium-Calcium Exchange, Inward Rectifier Potassium Current, and Residual {beta}-Adrenergic Responsiveness. Circulation Research. 2001; 88:1159–1167. [PubMed: 11397782]

44. Zhao Z, Wen H, Fefelova N, Allen C, Baba A, Matsuda T, et al. Revisiting the ionic mechanisms of early afterdepolarizations in cardiomyocytes: predominant by Ca waves or Ca currents? Am J Physiol Heart Circ Physiol. 2012; 302:H1636–H1644. [PubMed: 22307670]

45. Szabo B, Sweidan R, Rajagopalan CV, Lazzara R. Role of Na+:Ca2+ exchange current in Cs(+)-induced early afterdepolarizations in Purkinje fibers. J Cardiovasc Electrophysiol. 1994; 5:933–944. [PubMed: 7889233]

Highlights

- First recording of $I_{Na\text{-}L}$ during action potential with Ca^{2+} cycling
- Comparing $I_{Na\text{-}L}$ with three major K^+ currents in the same cell
- Novel finding of large $I_{Na\text{-}L}$ comparable to I_{Ks} and I_{Kr}
- Reveal significant role of $I_{Na\text{-}L}$ in action potential repolarization
- Interplay between $I_{Na\text{-}L}$ and Ca^{2+} dynamics causes EAD, DAD, TAP

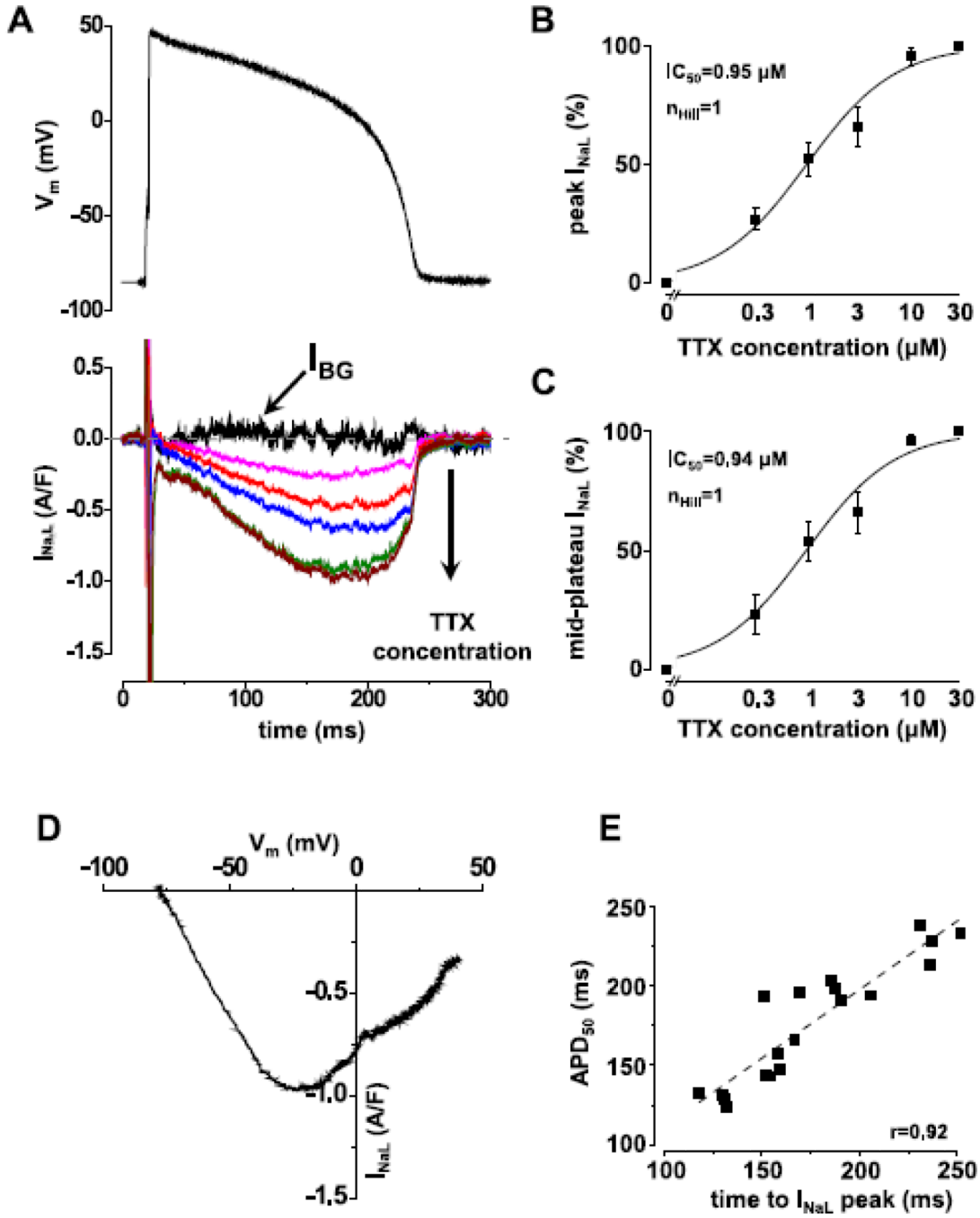

Fig.1. sAP-clamp recording of $I_{Na,L}$ as TTX-sensitive current in guinea pig ventricular myocyte

Panel A shows a representative set of $I_{Na,L}$ current recorded under sAP-clamp by using TTX. As the TTX concentration increases (0, 0.3, 1, 3, 10, 30 nM), larger fraction of $I_{Na,L}$ is visualized. B & C show the TTX concentration dependence of peak and mid-plateau current magnitudes (Mean±SEM, n=7cells/3animals). The Hill coefficient and IC_{50} values are the same at the peak and mid-plateau point, indicating the high specificity of TTX in blocking $I_{Na,L}$ within the concentration range examined. Panel D shows the dynamic I-V relationship of the full amount of $I_{Na,L}$ dissected out by 30 nM TTX plotted against the membrane

potential. Panel E shows a tight correlation between APD_{50} and the time to peak $I_{Na,L}$ (n=19cells/11animals). Similar correlations were observed for APD_{75} and APD_{90}.

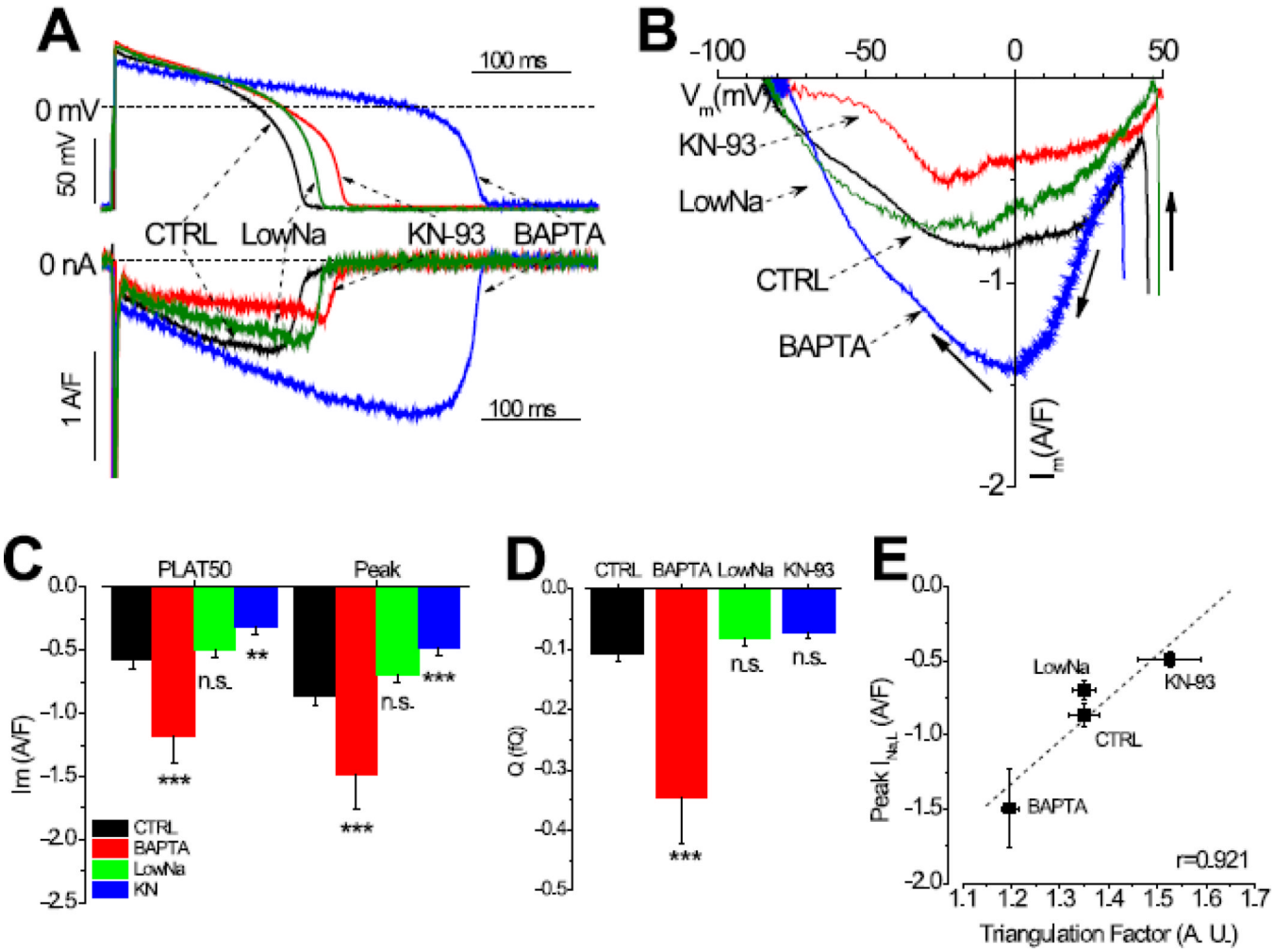

Fig.2. Modulation of I_{NaL} by Ca^{2+} and CaMKII

Panel A shows representative traces of $I_{Na,L}$ recorded in control cells (n=19cells/11animals), in BAPTA treated cells (n=11cells/5animals), in Low Na treated cells (n=7cells/3animals), and in 1 μM KN93 treated cells (n=10cells/5animals). Panel B shows the dynamic I-V relationship of $I_{Na,L}$ when the Ca^{2+} and CaMKII signaling were normal and altered by the above different interventions. Panel C & D show the total charge carried by $I_{Na,L}$ (Q_{Na}) and the peak current magnitude, respectively. Panel E shows a tight correlation between the amplitude of $I_{Na,L}$ and the triangulation factor of the AP shape, demonstrating the presence of non-equilibrium gating.

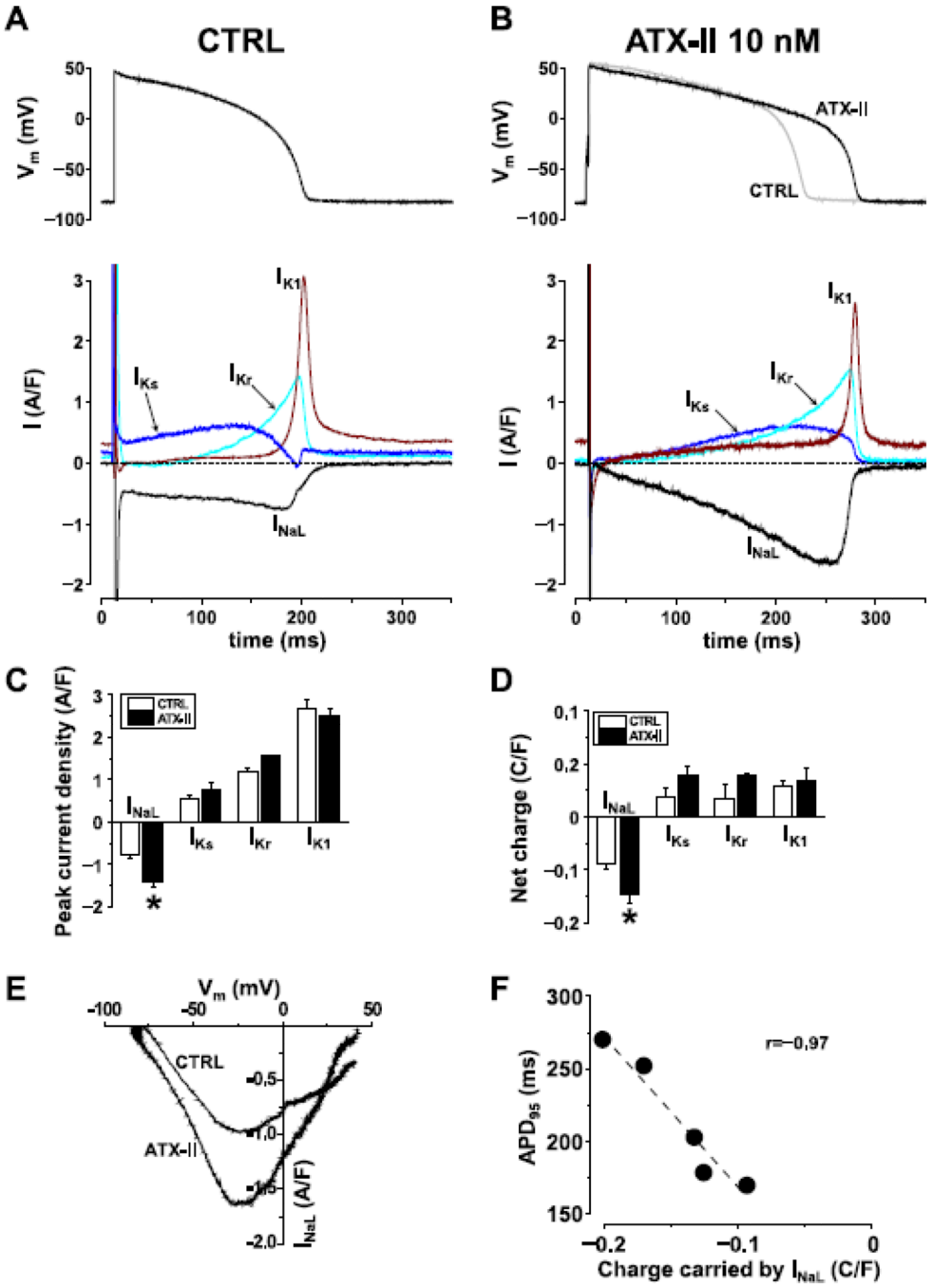

Fig.3. sAP-clamp Sequential Dissection of I_{NaL} and three major K^+ currents from the same cell

Representative traces of I_{NaL}, I_{Ks}, I_{Kr} and I_{K1} recorded from control cells (Panel A, n=6cells/5animals) and following facilitation by 10 nM ATX-II treatment (Panel B, n=5cells/3animals). ATX increased the peak current density (Panel C) and net charge (Panel D) without altering the K^+ currents. Facilitation with ATX-II did not alter the dynamic I-V relationship (Panel E). When AP was lengthened the net charge carried by the current was increased as is shown by the good correlation with APD_{90} (Panel F).

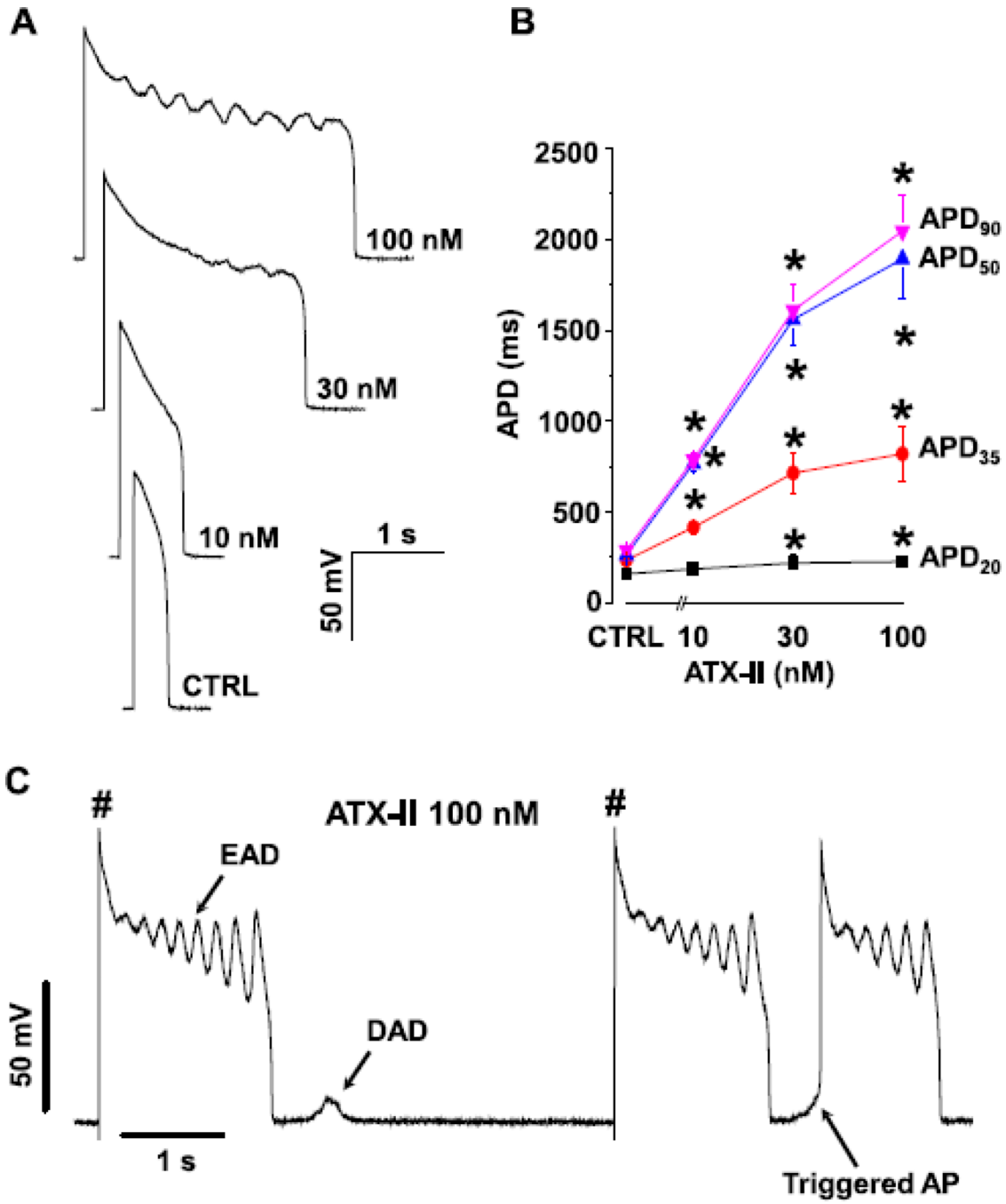

Fig.4. Effect of $I_{Na,L}$ on AP morphology

Panel A shows representative APs recorded in the presence of different ATX-II concentrations. Using ATX-II to upregulate I_{NaL} resulted in AP lengthening and generation of EAD. Panel B shows the concentration dependent AP lengthening effect of ATX-II at 0.2 Hz stimulation rate (n=6–11cells/6 animals). Panel C show the induction of various forms of arrhythmogenic APs (EAD, DAD, TAP) with ATX-II 100 nM in the same cell.

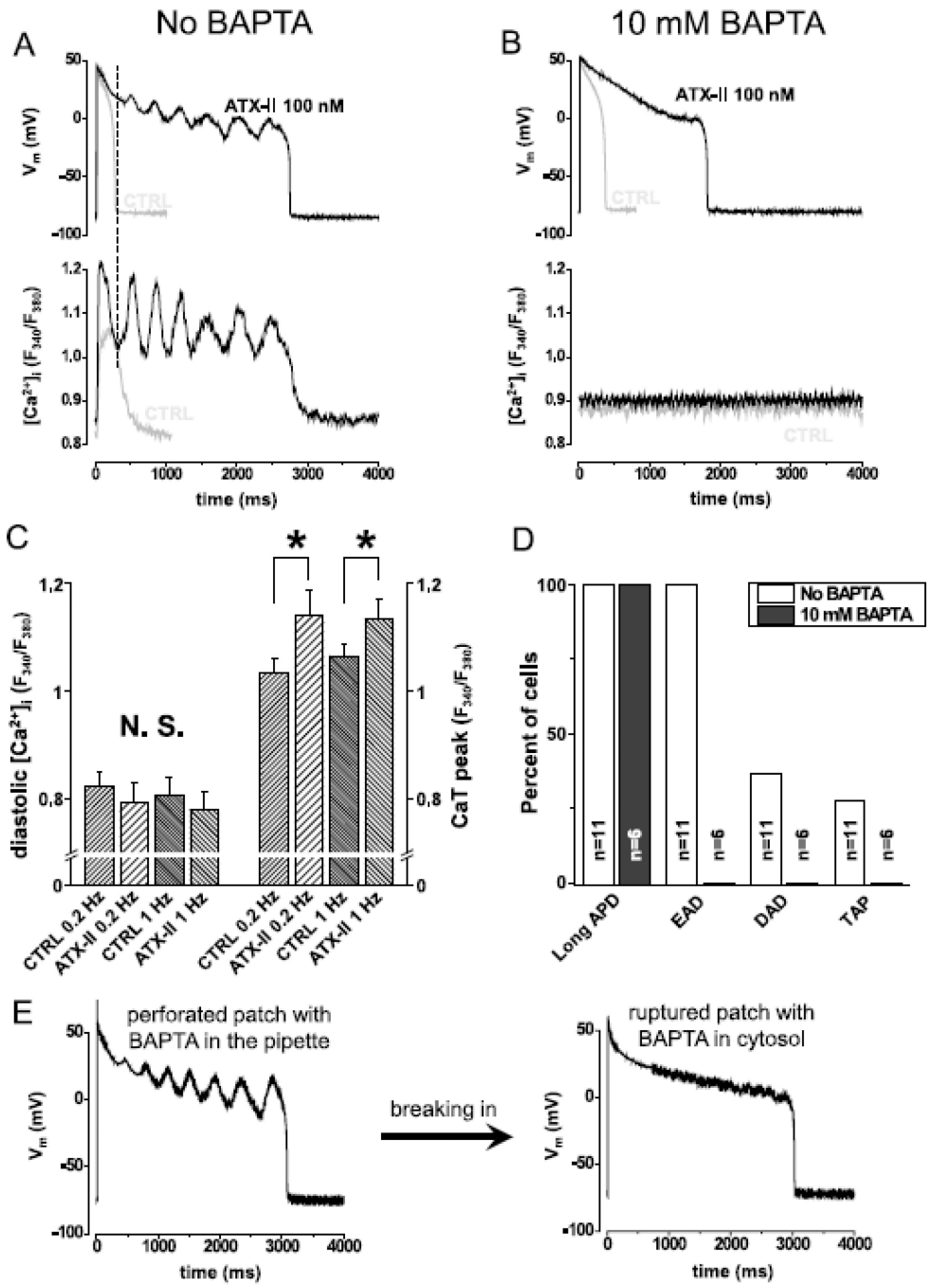

Fig.5. Spontaneous Ca^{2+} oscillation gives rise to EAD

Panel A shows simultaneous recording of AP (upper trace) and Ca^{2+} concentration (lower trace) under sAP-clamp (n=9cells/5animals). Grey and black lines show traces recorded in the absence and the presence of 100 nM ATX-II, respectively. ATX-II lengthened APD but EADs were seen only when Ca^{2+} was not buffered. Dashed line in panel A shows that the rise in Ca^{2+} signal precedes the turning point of membrane potential indicating that Ca^{2+} drives EAD. Panel B shows that when Ca^{2+} was clamped to 100 nM using BAPTA (n=6cells/3animals), ATX-II lengthened AP but no EAD was observed (grey line control, black line ATX-II). Statistical analysis of the Ca^{2+} transients (Panel C,) reveal that systolic, but not diastolic Ca^{2+} concentration was increased by ATX-II at 0.2 Hz (n=9cells/5animals)

and 1.0 Hz (n=8cells/5animals) pacing rate. Panel D shows the percent of cells developing various forms of arrhythmogenic APs in the presence of 100 nM ATX-II. When Ca^{2+} cycling was not buffered (n=11cells/6animals), all cells developed long APD and EADs and some developed DADs and TAPs. When Ca^{2+} was buffered with BAPTA (n=6cells/3animals), the cells developed long APD, but no EAD, DAD or TAP was seen.